Chapter 4

Preparation of Immunosensor Platforms

4.1 Introduction

In recent years, extensive work has been done on developing high-sensitivity electrochemical biosensors by increasing surface-to-volume ratio and conductivity. Thus, the electrochemical biosensor has gained significate interest in addressing the need to develop rapid, low cost and point-of-care diagnostic systems [113-115]. There have been three areas of interest while addressing the challenges in electrochemical biosensors (i) identifying a suitable choice of materials that severs the objective of achieving higher biocompatible nature with conducting characteristics, (ii) finding appropriate methods for binding these on substrates, and (iii) controlling thickness at the surfaces. In the past, a range of vacuum and non-vacuum-based methods such as chemical vapor deposition [121], physical vapor deposition [122], electrodeposition [123], sol-gel, and many other ways have been used for the deposition of thin films and coatings [119-120]. These provide unique characteristics and control over physicochemical properties, but the thickness may differ for different deposition methods.

The surface modification has also been used to achieve functionalization or deposition of molecular layers through self-assembly had also provided desired binding sites at the surfaces [121-123]. Self-assembly is a spontaneous process that allows the assembly of molecules with a specific binding affinity toward substrates, making better control over the surface thickness possible [118].

The Langmuir-Blodgett process has been very commonly used for depositing thin films of organic monomers with better control of thickness [127], [128]. The usefulness of Langmuir–

Blodgett films has been demonstrated in interfacial nano-architectonics with biomolecules [129], materials, living objects [130], optical gas sensing [131], polymer light-emitting diodes [132], single-molecule nanomagnets [133], and biosensors [134], [135]. The deposition of Langmuir–Blodgett film involves the creation of a well-ordered structure of a compact Langmuir monomolecular layer at the air-water interface and subsequently transferring the highly oriented thin film layer onto substrates by the vertical dipping method [136]. This enables the preparation of 2D materials coatings of a single molecular layer with the possibility of incorporating a range of molecules and nanoparticles [137], [138]. Thus, there is limited scope for metallic nanoparticles or nanocomposites of polymeric, metallic, and semiconducting materials due to their relatively higher mass density with molecules participating in this process. However, nanocomposites of polymeric, metallic, carbon-based materials, and semiconducting materials [139]–[144] show application in many filed due to their size [145], surface charge [146], functional group [126], optical response [125], and conducting behavior [147].

Despite several advantages and valuable properties of these nanomaterials, a significant challenge has been poised to graft their stable thin films without using intermediate additive functional groups [148], [149]. However, the use of these groups has resulted in a compromise of the natural characteristic properties of these uniquely designed materials [150]. Thus, different approaches such as energy assistive deposition [122], functionalization of substrate material [119], and modification of surface properties of nanomaterials [151] have been adopted to make them suitable for coatings. Surface modification has been an attractive choice for either preparing substrate surfaces suitable for binding the nanomaterial or anchoring the functional groups on nanomaterial surfaces to make them adhere to other substrates. Several reports have demonstrated successful modification of substrate surface

properties by ionic or thiol functionalization and self-assembly [152]–[155]. In addition, over-achieving better adhesion of nanomaterials on surfaces and improving biocompatibility with retention of surface conductivity has also been a challenge in making suitable platforms for electrochemical bio-sensing. There are several deciding factors to it, but controlling the thickness of depositing film could result in high conductivity with retention of the biocompatibility attribute. Langmuir Blodgett film deposition methods are advantageous over the others in depositing a monolayer of the desired material without compromising surface characteristics along with its lower energy consumption and convenient instrumental operation [156]. The essential condition for the development of a stable and uniform LB film is that the material must be hydrophobic in nature or functionalized with hydrophobic groups [157]. The functionalization of the surface is prone to lesser conductivity or alteration in the natural characteristic properties of the nanomaterials.

This study had formulated a unique design where a positively charged monomer of a conductive polymer has been electro-polymerized on the surface of negatively charged metallic, metallic oxide nanoparticles. The conductive polymer matrix facilitates the stacking of the nanoparticles and prevents their aggregation without decreasing their conductivity [146], [158], [159]. Several polymers, such as polyaniline, polypyrrole, polythiophene, etc., have been reported so far, aiding conductivity. Polyaniline (PANI) and its different composites were among the most studied hybrid materials due to their low cost, modification flexibility, and accessible synthesis route [160], [161]. The polymer has superior conductivity and electron transfer ability, making it an excellent candidate for electrochemical analysis [162]–[164]. In addition to it, PANI also possesses an irregular porous structure that favors its doping potential with metallic nanomaterials, thereby enhancing its electrochemical sensing properties [137], [165], [166]. The other advantage of polyaniline (PANI) is having

a reactive -NH- group in the polymer chain, imparting the system's hydrophilic character. However, PANI suffers from a few limitations, mainly stability, and low processing ability addressed in ample research by doping with various nanoparticles [159], [167]–[169].

In the first part of this study, titanium dioxide (TiO_2) nanoparticles were chosen and doped in aniline. The electrochemical polymerization process was used for synthesizing PANI-TiO_2 nanocomposites. Many methods have been used to synthesize PANI-TiO_2 nanocomposites, such as oxidative chemical polymerization of aniline in the presence of TiO_2, polymerization using reverse mice, and physical mixing [170]–[172]. However, all these methods do not provide control over depositing a single molecular layer; hence the responses are as bulk properties, without precision control over molecular layers and thickness of the films. Thus, appropriate conditions were optimized to prepare low-density dispersions of PANI-TiO_2 in suitable solvents for the deposition of polyaniline-TiO_2 nanocomposite thin films by the Langmuir-Blodgett process. This study introduced a scheme in which PANI-TiO_2 nanocomposites were synthesized by electropolymerization [173] of a mixture of aniline and TiO_2 nanoparticles on an ITO substrate. Further, the electropolymerized PANI-TiO_2 nanocomposites were dissolved in a solution of N-methyl-2-pyrrolidone (NMP) and isopropanol for monolayer deposition through the LB process. This may provide an advantage in increased conductivity of nanocomposites, higher charge transfer on the electrode surface, and uniform functionalization sites for binding antibodies. The prepared LB film of PANI-TiO_2 was functionalized by immobilizing monoclonal anti-glutamate antibodies and used to detect MSG through an electrochemical process. In the second part, from the family of metallic nanoparticles, GNPs were chosen due to their exceptional conductivity as well as high stability over a wide range of pH and temperatures. Due to electrostatic forces of attraction, a stable nanocomposite of PANI/GNP has been obtained,

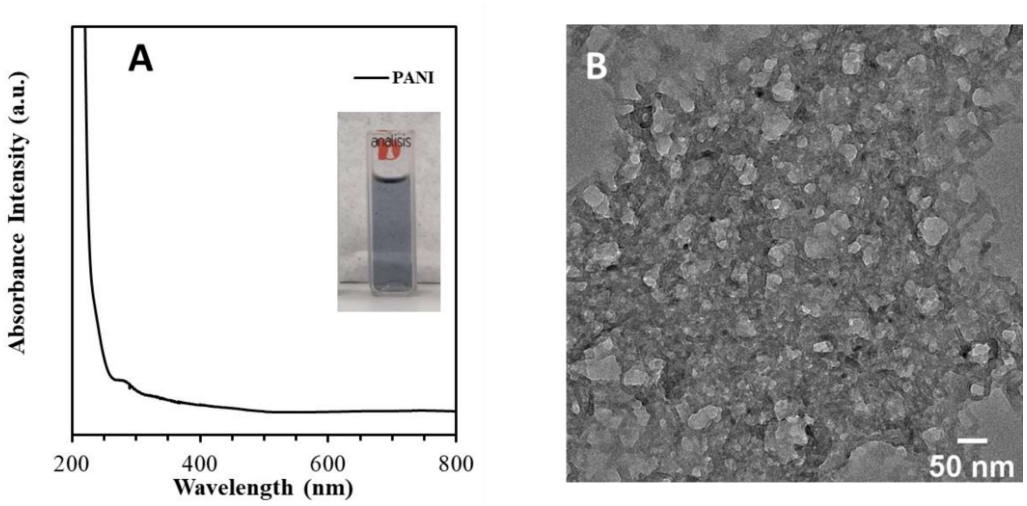

Figure 4.1: (A) *UV-vis spectrum PANI at 290 nm and optical image PANI colloid disperses* ***(B)*** *TEM image of PANI.*

which is insoluble in water. This study implemented a unique strategy where PANI-GNP nanocomposites were synthesized via electro-polymerization onto ITO. The LB film of PANI-GNP nanocomposite results in the amplification of conductivity and has been used as a working electrode in developing electrochemical biosensors to quantify MSG.

4.2 Electrochemical Synthesis

4.2.1 Synthesis of PANI Through Electrochemical Polymerization of Aniline

Polyaniline (PANI) is one of the most widely used conductive polymers having a reactive -NH- group in the polymer chain, imparting the system's hydrophilic character. However, PANI suffers from a few limitations, mainly stability, and low processing ability, which have been addressed in ample research by its electro-polymerization. The electro-polymerization of the aniline monomer was carried out in a three-electrode cell. The ITO-coated glass was used as the working electrode, a platinum wire as the auxiliary electrode, and Ag/AgCl as a reference electrode.

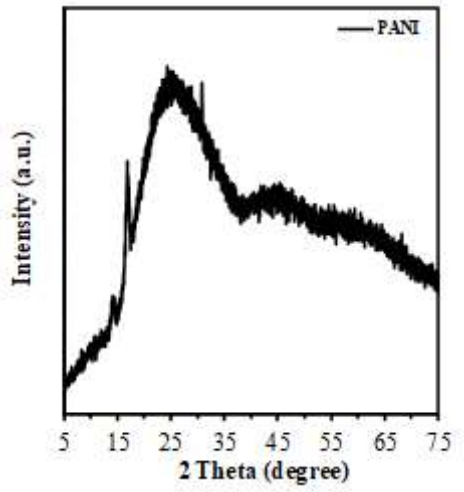

Figure 4.2: *XRD pattern of PANI.*

For the electrochemical polymerization, a solution of 500 µl of sulfuric acid and 91 µl of aniline in 10 ml DI was used. The mixture is sonicated for 30 min. Electro-polymerization was achieved by sweeping the potentials in the range from -0.3 V to 0.9 V for 21 cycles with a sweep rate of 30 mV s^{-1} and continuous purging of 99% pure nitrogen gas. The PANI was collected by physical removal from the ITO substrate. The collected sample is dried overnight in a vacuum oven at 45º C and stored for the LB film deposition process. In the experiment used, sulfuric acid, hydrogen peroxide, ammonia, aniline monomer, hydrochloric acid, and potassium dichromate were purchased from Sigma-Aldrich, and all the experiments were performed with the use of deionized (DI) water from a Millipore system (~18.2MΩ cm).

4.2.2 Physicochemical Characteristics Of Electrochemically Polymerized Aniline

The UV-visible spectral measurements were carried out using a Shimadzu UV-visible spectrophotometer (Tokyo, Japan). Figure **4.1 (A)** shows the UV–vis absorbance spectra of PANI. The spectral optical absorption peak was at 290 nm for PANI. Figure **4.1 (B)** shows

the TEM image of PANI, which confirms Successful PANI polymerization from an aniline monomer. The XRD pattern of PANI shows peaks corresponding to crystallite structures associated with (100) and (110) planes [JCPDS No. 53–1718] in **Figure 4.2.**

4.2.3 Preparation of TiO_2 Nanoparticles

TiO_2 nanoparticles were synthesized by the sol-gel method using titanium isopropoxide, isopropanol, and nitric acid in a quantity of 7.4 ml, 91.1 ml, and 1.5 ml, respectively, and were mixed under strong magnetic stirring. Then the solution was stirred at a temperature of 60°C for one h, which led to the formation of white powder, which was annelid in the ambient atmosphere to improve its crystalline nature. The synthesized TiO_2 nanoparticles were characterized by obtaining their XRD pattern and UV-vis spectra and results are shown in **Figure 4.3**.

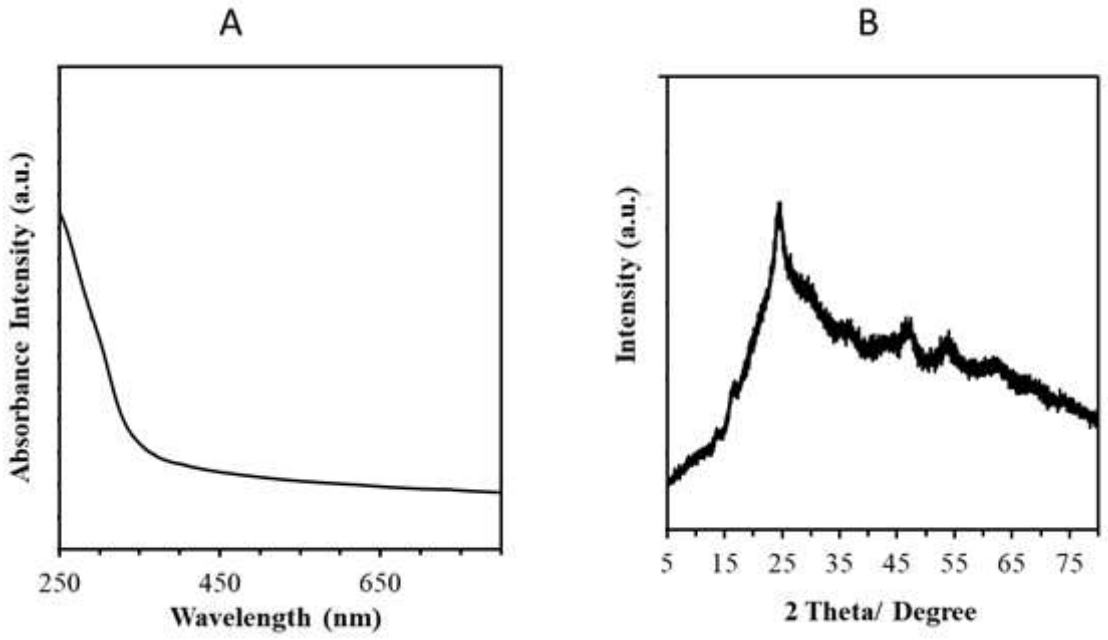

Figure 4.3: *(A) UV-vis spectrum of TiO_2. (B) XRD pattern of TiO_2.*

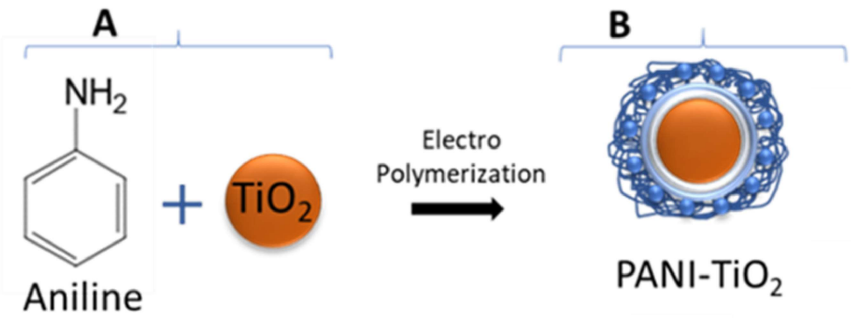

Figure 4.4: *(A) Schematic representation of electrochemical polymerization of aniline and TiO_2. (B) Diagrammatic illustration of PANI-TiO_2 nanocomposites.*

4.3 Synthesis of PANI-TiO_2 Through Electrochemical Polymerization

4.3.1 Synthesis Process

Electropolymerization of TiO_2 nanoparticles containing protonated aniline was done in the acidic pH using a three-electrode system on ITO electrodes, as shown in the schematic representation in **Figure 4.4**. Electrochemical polymerization was performed using GAMRY Reference 3000, potentiostat/ galvanostat/ZRA, USA. For the electrochemical polymerization, a solution of 500 µl of sulfuric acid and 91 µl of aniline in 10 ml DI was used. Further, 100 mg TiO_2 was added to this prepared solution and sonicated for 30 min. Electro-polymerization was achieved by sweeping the potentials from -0.3 V to 0.9 V for 21 cycles with a sweep rate of 30 mV s^{-1} and continuous purging of 99% pure nitrogen gas. The PANI-TiO_2 nanocomposites were collected by physical removal from the ITO substrate. The polymerization reaction was performed by applying voltage from -0.3 V to 0.9 V in each cycle for successive 21 cycles. The cyclic voltammetry response of each cycle during electrochemical polymerization was recorded, and the results are shown in **Figure 4.5**.

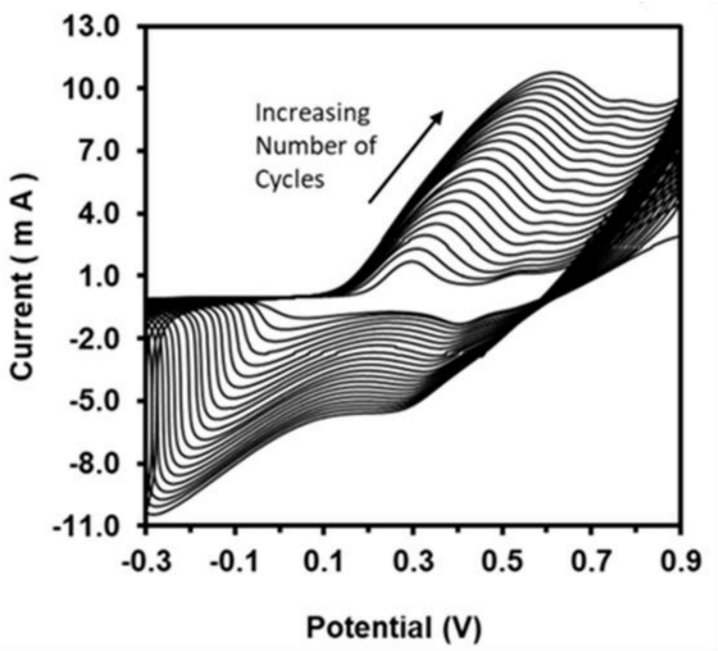

Figure 4.5: *CV response of electrochemical polymerizing PANI-TiO_2 for successive 21 cycles.*

4.3.2 Physico-chemical Characteristics of PANI-TiO_2

A fine powder of PANI-TiO_2 was collected from the ITO surface after the completion of electropolymerization and dissolved. PANI-TiO_2 nanocomposite began a homogenous and stable dispersion in NMP and isopropanol. The relatively low density of the homogenous solution enabled the preparation of a floating nanocomposite monolayer on the water as a steady air-water interface. A transmission electron microscope (JEOL JEMCX11, Japan) at an operating voltage of 150 kV was used to check the deposited film's surface characteristics. The samples were prepared after drop-casting the diluted solution over the carbon-coated copper grid with 400 mesh.

The PANI-TiO_2 nanocomposite dispersed solution was drop cast on a copper grid, and TEM images of the films were acquired, as shown in **Figure 4.6 A**. A high-resolution TEM image was acquired for individual single particles of TiO_2, and the result is shown in **Figure 4.6 B**.

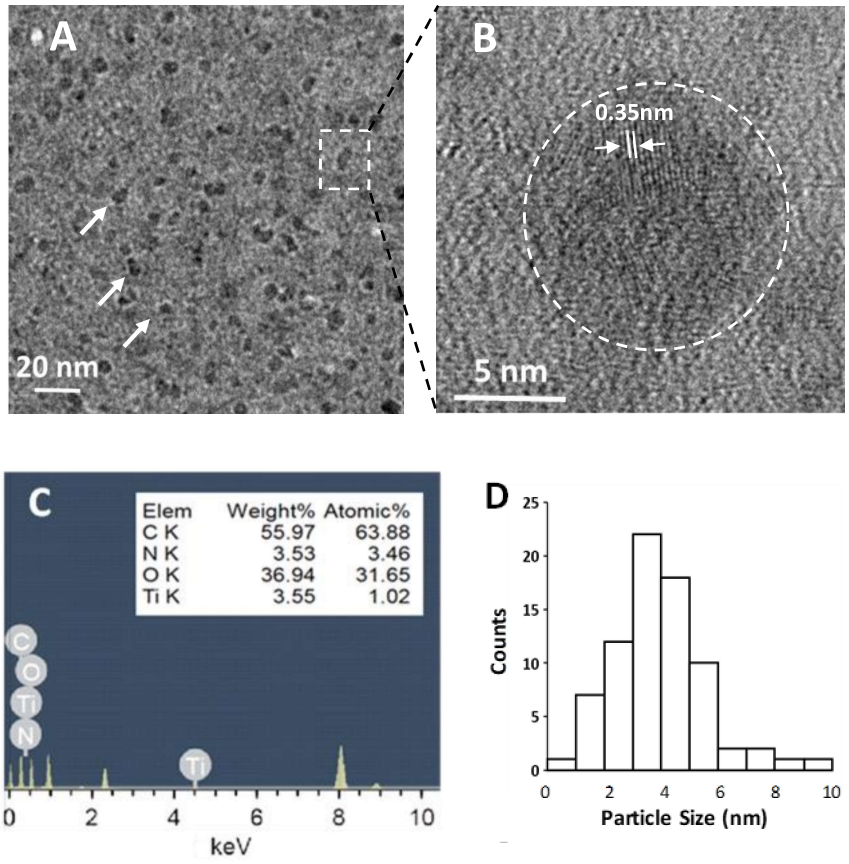

Figure 4.6: *(A) TEM image of PANI-TiO_2, (B) High-resolution TEM images showing lattice pattern of TiO_2, (C) Energy dispersive X-ray analysis of PANI-TiO_2 nanocomposites showing the relative atomic proportion of different elements present in nanocomposites, (D) bar graph of TiO_2 nanoparticle size distribution in PANI-TiO_2.*

A systematic titania atomic arrangement was observed having an interatomic distance of ~ 0.35nm, corresponding to the anatase (101) crystalline plane. The presence of TiO_2 has further confirmed with energy dispersive analysis at the same spot where the TEM analysis was performed. A peak corresponding to TiO_2 was obtained in the EDX pattern, as shown in **Figure 4.6C**. This confirmed the presence of TiO_2 in the PANI-TiO_2 nanocomposite. Further J-image analysis of uniformly distributed TiO_2 in **Figure 4.6A** was performed. The results of the ImageJ analysis are shown as a bar graph of particle size distribution in **Figure 4.6D** with an average calculated size of ~ 5nm.

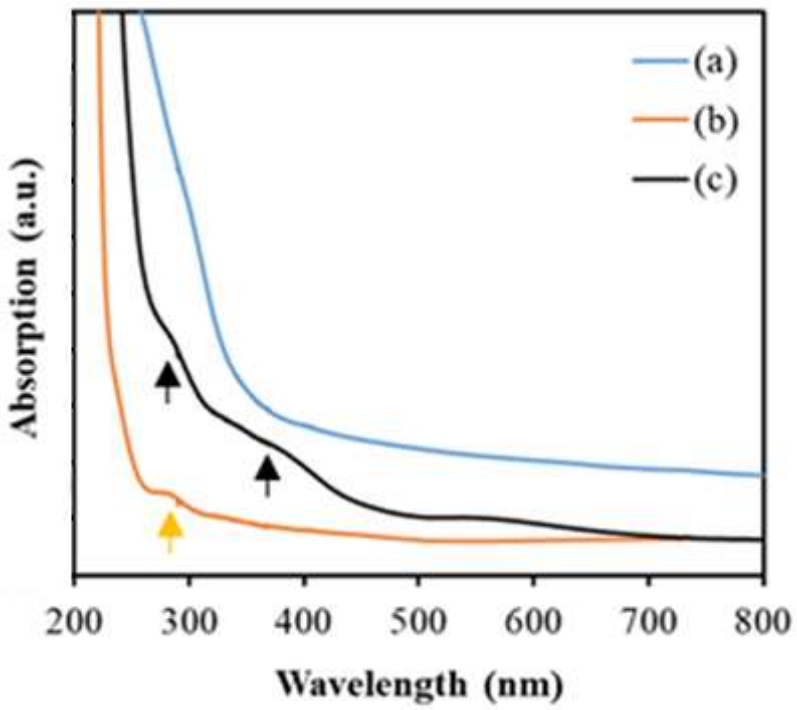

Figure 4.7: *UV-vis spectra of (a) TiO_2, (b) PANI, and (c) PANI-TiO_2.*

UV-vis spectra of PANI and PANI-TiO_2 in NMP solvent were obtained, and the results are shown in **Figure 4.7**. UV-vis absorbance spectra of TiO_2, PANI, and PANI-TiO_2 composites. The spectral optical absorption peak was at 290 nm for PANI, peak at 320 nm for TiO_2, and peaks at 290 nm and 380 nm for PANI-TiO_2 nanocomposites. This could be attributed to the π–π* and polaron–π* transition in the conducting PANI [174], [175]. The absorption edge was shifted towards the longer wavelength side for PANI-TiO2 nanocomposite might be due to the coordinate complex formation between TiO2 nanoparticles and PANI [176].

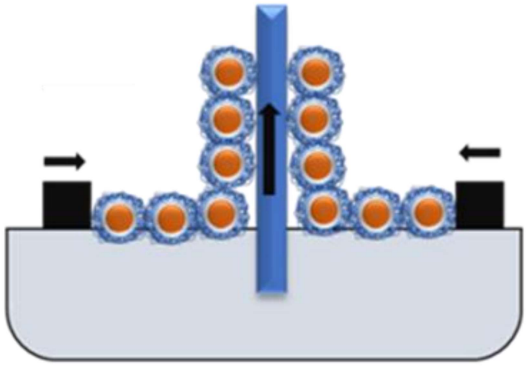

Figure 4.8: *Schematic illustration of L-B film deposition of PANI-TiO_2.*

4.3.3 Deposition of PANI-TiO_2 Nanocomposite LB film

A schematic representation of LB film deposition is shown in **Figure 4.8**. In this, the ITO glass was cleaned in a solution of hydrogen peroxide, ammonia, and DI water in the ratio of 1:1:5 at 75^{o} C for 30 minutes and then rinsed with ethanol and dried with the help of 99% pure nitrogen. The trough (mini-trough (KSV-NIMA, Finland) was cleaned with ethanol, followed by DI, and dried using nitrogen gas to obtain a contamination-free subphase for monolayer. To prepare LB film of PANI-TiO_2 nanocomposite, 1 mg/mL PANI-TiO_2 nanocomposite was dissolved in a solution of NMP and isopropanol in a ratio of 1:9 and was probe sonicated for 30 minutes. Then 200µL of this solution was spread using a Hamilton microsyringe over the trough, containing ultrapure Milli-Q (pH 6.00) water. NMP having a higher density than Milli-Q water got settled at the bottom of the trench, while isopropanol, being volatile, left the system [177]. After approximately 30 min, the composite material remained on the water's surface. PANI and PANI-TiO_2 solutions were gently dispersed on the water interface, and the pressure-area (p-A) isotherms were recorded during the PANI-TiO_2 Langmuir monolayer formation at the water-air interface (**Figure 4.9**).

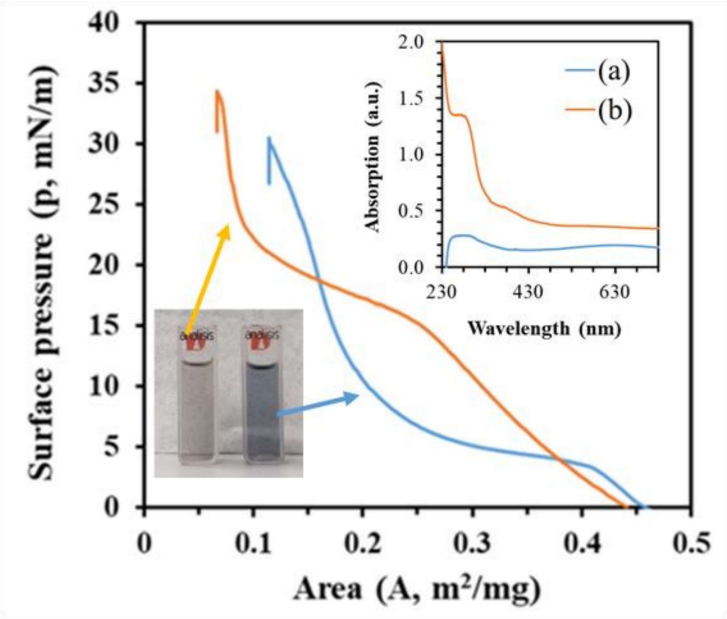

Figure 4.9: *Surface pressure - area (p-A) curve during optimizing of LB film deposition conditions where (a) PANI and (b) PANI-TiO_2; inset images show UV-vis spectra of (a) PANI and (b) PANI-TiO_2 along with optical images of their suspension in a solvent.*

The water surface available area in these isotherms was measured in m^2 with the dispersed quantities of PANI and PANI-TiO_2 in mg^{-1}. The PANI-TiO_2 isotherm showed a reduction in surface area from 0.45 to 0.24 m^2/mg, resulting in a linear increase in the pressure from 0 to 15 mN/m, whereas a further decrease in the area showed a transition in the rate of change in the surface pressure. This indicated a shift from a single layer to a multilayer of molecules. Thus, for depositing LB film of PANI-TiO_2, 10 mN/m pressure was chosen. During this transition, the nanosheets of PANI-TiO_2 float on water due to the surface tension making a steady water-air interface [178]. For transferring water-air interface LB films of PANI-TiO_2 on the ITO electrode, chemically pretreated ITO substrate was clamped to the dipper, and films were deposited on substrates using the vertical dipping at a speed of 2 mm min^{-1}, as schematically shown in **Figure 4.8**.

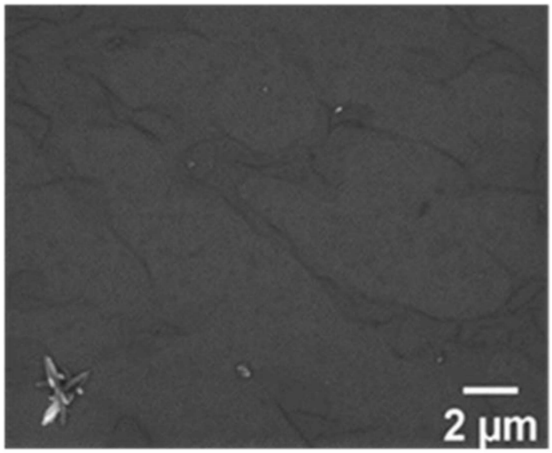

***Figure 4.10**: SEM image of PANI-TiO_2 LB film.*

4.3.4 Characteristics of PANI-TiO_2 Nanocomposite LB films

Field emission scanning electron microscopy (FE-SEM with the use of Zeiss sigma VP FE-SEM, Germany) was acquired, and the result is shown in **Figure 4.10**. SEM images of LB films of PANI-TiO_2 on the ITO electrode showed a topological view and confirmed the formation of uniform structures of PANI-TiO_2 across the surface.

The X-ray diffraction pattern of PANI, TiO_2, and PANI-TiO_2 films on glass substrates was analyzed by an X-ray diffractometer, and the results are shown in **Figure 4.11**. The XRD pattern of PANI shows peaks corresponding to crystallite structures associated with (100) and (110) planes [JCPDS No. 53-1718]. The XRD pattern of TiO_2 shows distinct well, defined peaks that could be indexed to a tetragonal structure with an anatase phase. XRD peaks of TiO_2 film were observed at 24.7°, 37.46°,47.36°,54.00°, and 62.08°, corresponding to crystal planes (101), (004), (200), (105), and (204), respectively [179]. All these positions of TiO_2 peak in XRD spectra were attributed to the anatase structure of TiO_2 (JCPDS-73/1764). The XRD pattern of PANI-TiO_2 shows distinct, well-defined peaks that could be

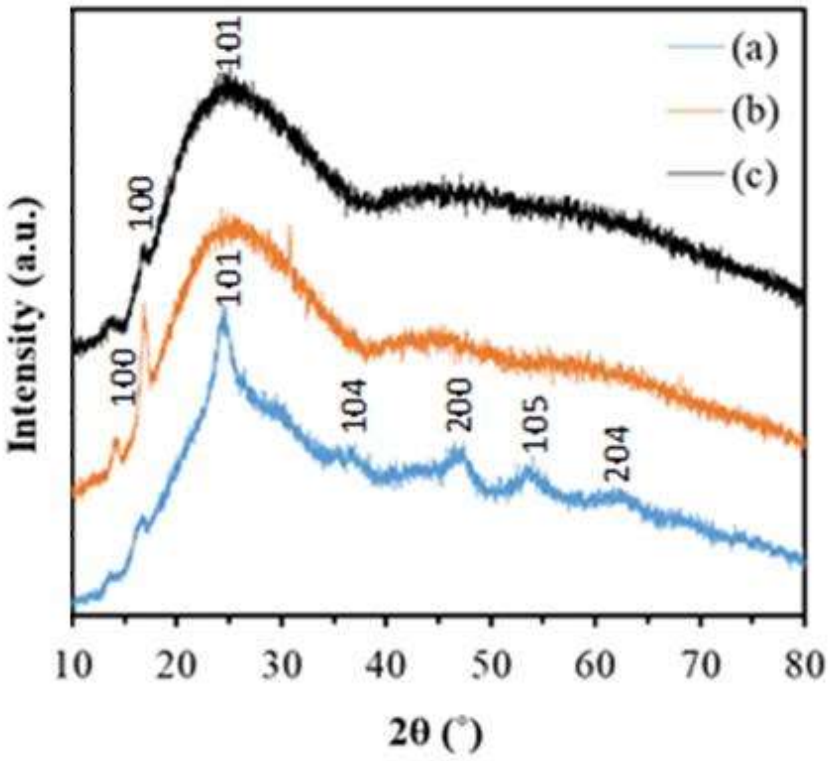

Figure 4.11: *XRD pattern of (a) TiO_2, (b) PANI, and (c) PANI-TiO_2.*

indexed to a tetragonal structure with an anatase phase. The background glass's amorphous characteristics dominated in the XRD peak for the condition; however, a small peak in the XRD pattern of TiO_2 film was observed at 24.7°, which corresponds to crystal planes (101) of the anatases phase. Compared to TiO_2, the PANI- TiO_2 diffraction peaks were revealed to broaden and decrease the intensity, and this may be due to the polymerization of PANI onto the TiO_2 in the composites [174].

The PANI-TiO_2 LB film deposited on the ITO substrate was further characterized by X-ray photoelectron spectroscopy [180], and the results are shown in **Figure 4.12**. A broad scan XPS spectrum of TiO_2 nanoparticles and PANI-TiO_2 LB film was obtained. XPS elemental

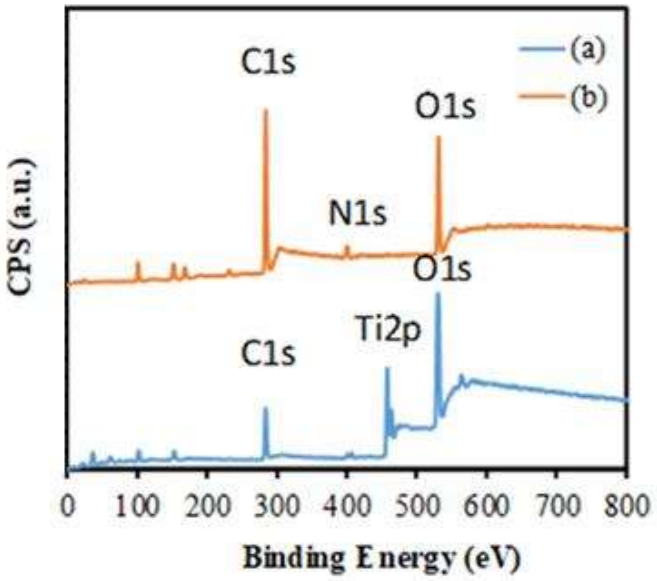

Figure 4.12: *Wide scan X-ray photoelectron spectra of TiO_2 and PANI-TiO_2 film surface.*

analysis of PANI-TiO_2 showed 73%, 21.9%, 4.7%, and 0.5% atomic percentage proportions of carbon, oxygen, nitrogen, and titanium, respectively, as shown in the figure. Relative proportions of different elements at the surface were calculated from these spectra. The ratio of Ti/O at the surface of TiO_2 nanoparticles in XPS broad spectra was 0.24. This O/Ti ratio was decreased in PANI-TiO_2, and the appearance of the peak corresponding to nitrogen is shown in the XPS wide scan spectra. This confirmed the aniline polymerization on the surface of TiO_2.

4.4 Synthesis of PANI-GNP Through Electrochemical Polymerization

4.4.1 Synthesis Process

The GNP in this section was used as synthesized in section 3.4 of the last chapter. **Figure 4.13** shows UV-vis spectra along with a TEM image for measuring the particle size of the used GNP.

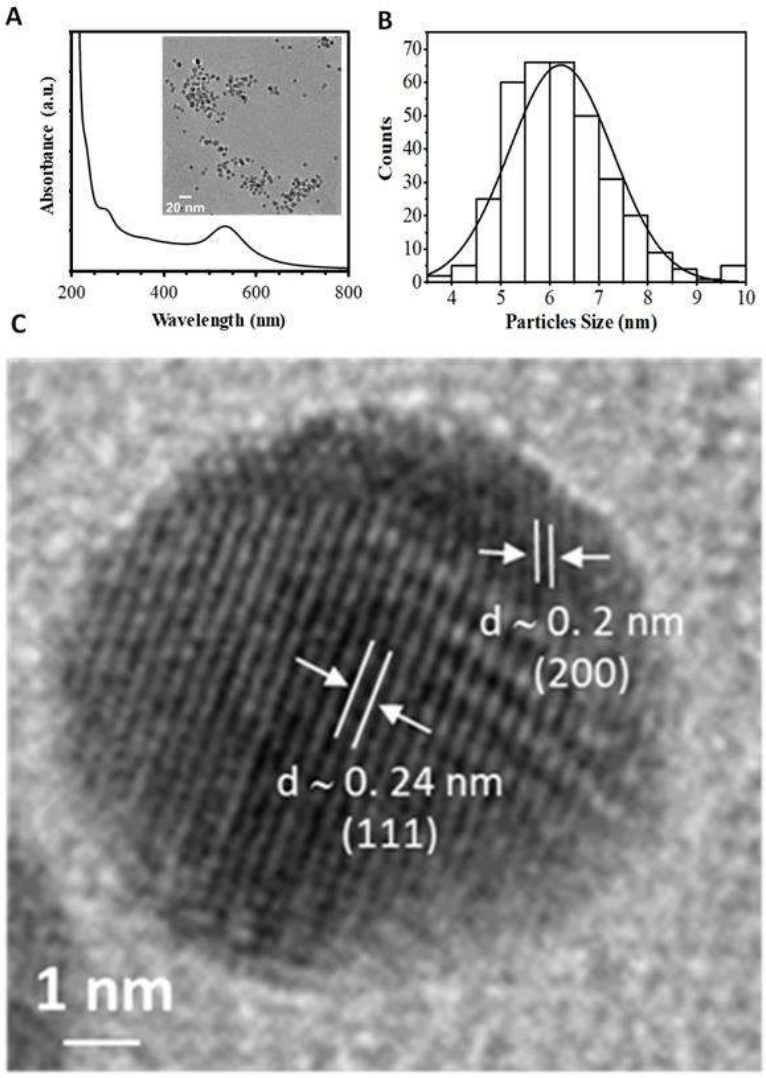

Figure 4.13: *(A) UV-vis spectrum of GNP colloidal suspension and TEM image of GNP, (B) Size distribution curve of GNP in TEM image with Image J software. (C) TEM image of single GNP.*

The synthesized gold nanoparticles were prepared using LiBH4 as a reducing agent without any stabilizers [90]. The GNP colloid disperses red color, which is confirmatory to its synthesis, and its UV-vis spectrum shows λ_{SPR} at 535 nm (Figure 4.13 A). TEM image study of GNP has also been shown in the inset of Figure 4.13 A, indicating the uniform distribution of spherical gold particles.

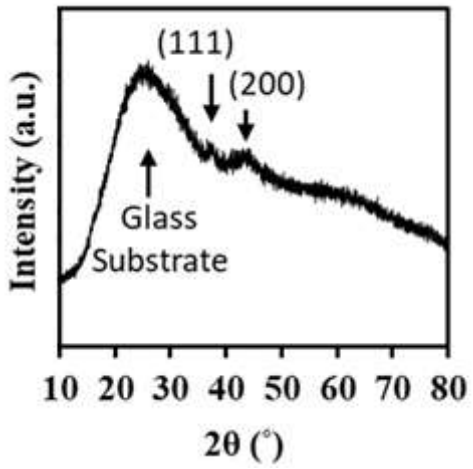

Figure 4.14: *XRD spectrum of GNP film on a glass substrate.*

J-image software has been used to process the TEM image for measuring the size of the particles. **Figures 4.13 B** demonstrates an average diameter of ~ 6 nm taking into account almost 347 Gold nanoparticles in a single image, as indicated in the size distribution curve of the ImageJ software. The curve has a gaussian-like distribution with a full-width half-maxima value of ~ 2.5 nm. **Figures 4.13 C** shows the high-resolution TEM image having interplanar spacing (d) ~ 0.24 nm for the (111) plane and ~ 0.20 nm for the (200) plane. XRD analyses of GNP have been shown in **Figure 4.14**. The XRD pattern showed the broad intensity of peaks due to the low concentration of GNPs in the film. The spectrum illustrates two distinct characteristic peaks at the 2θ value of 38.42° and 44.38°, which correspond to (111) and (200) crystallographic planes, respectively. The position of the GNP peak in the XRD spectrum is attributed to the face-centered cubic structure of GNP.

The observed results coincide with the previous literature (JCPDS 65-2870), and also synchronizes with the outcomes of TEM analysis. Further, the electrochemical polymerization of the aniline monomer with chemically synthesized GNP was carried out in a three-electrode electrochemical cell. ITO-coated glass, platinum wire, and Ag/AgCl were

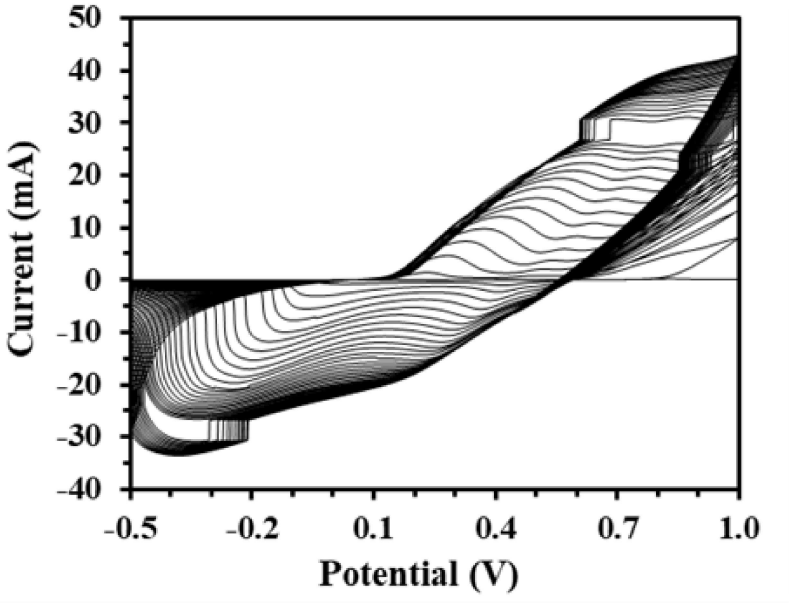

Figure 4.15: *Electrochemical polymerization of aniline monomer in GNP colloidal suspension and CV response during electrochemical polymerization for 35 cycles.*

used as working, auxiliary, and reference electrodes, respectively. A solution of 500 µl of sulfuric acid and 91 µl of aniline in 10 ml DI was taken for the electrochemical polymerization. Further, 1 ml GNP was added to this prepared solution and sonicated for 30 min. Electro-polymerization was achieved by sweeping the potentials from -0.3 V to 0.9 V for 35 cycles with a sweep rate of 30 mV s^{-1} with continuous purging of 99% pure nitrogen gas. In summary, aniline was added to the colloidal suspension of GNP and was allowed to interact in a time progression way. This mixture was allowed to interact for 60 min and then was used for the electropolymerization in the presence of sulfuric acid using 35 cycles of CV ranging from -0.3V to + 0.9 V, as shown in **Figure 4.15**.

4.4.2 Physico-chemical Characteristics of GNP-PANI

The PANI-GNP nanocomposites were collected by physical removal from the ITO substrate. EDX analysis of PANI-GNP was performed, and the results are shown in **Figure 4.16**. In the EDX pattern, the % proportion of gold was 5.9 weight %, confirming the presence of GNP

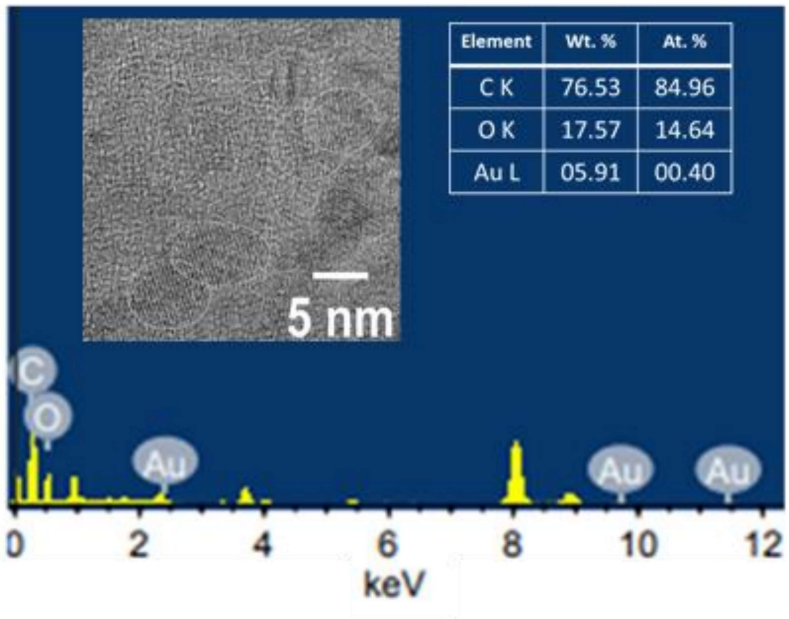

Figure 4.16: *Energy-dispersive X-ray analysis of PANI-GNP film surface showing the relative atomic proportion of different elements present in the LB film (inset image is high-resolution TEM of PANI-GNP).*

within the PANI matrix. The TEM image in the inset of the figure reveals the presence of spherical shaped and uniform distribution of GNP inside the PANI matrix with an average particle diameter of ~ 6 nm in the nanocomposite. Electrochemically deposited PANI-GNP nanocomposite on ITO was physically collected and dissolved in a solvent prepared by mixing 10 % V/V NMP in 90 % IPA. PANI-GNP nanocomposite forms a homogenous and stable dispersion in NMP and isopropanol.

X-ray diffraction (XRD) patterns were taken by Rigaku mini Flex-600 X-ray diffractometer with Cu Kα radiation (λ=1.5418 Å). The scan was carried out at a 2°/min speed and a 2θ range from 5^o to 80^o. The collected nanocomposite material solution was drop cast on a glass surface for acquiring XRD spectra. Characteristic peaks at the 2θ value of 15.4^o and 26.3^o in XRD spectra of PANI correspond to (100) and (200) planes (**Figure 4.17**).

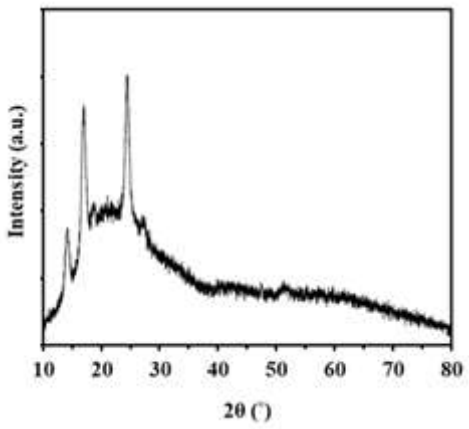

Figure 4.17: *XRD pattern of PANI-GNP on a glass substrate.*

4.4.3 Deposition of GNP-PANI-TiO_2 Nanocomposite LB film

The schematic representation of LB film deposition of GNP-PANI is shown in **Figure 4.18.** For this, a solution of concentrated sulfuric acid and hydrogen peroxide (35%) in the ratio of 3:1, commonly known as a 'piranha cleaning solution,' was used to clean the ITO glass for 30 seconds and then rinsed with ethanol and dried with the help of 99% pure nitrogen. The trough (mini-trough) (KSV-NIMA, Finland) was washed with ethanol followed by DI and dried using nitrogen gas to confirm a contamination-free subphase for the monolayer. A solution of 1 mg/mL PANI-GNP nanocomposite and N-methyl-2-Pyrrolidone (NMP) was prepared and probe sonicated for 30 min at an interval of 2 min. The resulting solution was diluted with isopropanol in a ratio of 1:9 and was sonicated again before use. 200 µl of the resulting solution was evenly spread using a Hamilton microsyringe over the trough containing ultrapure Milli-Q water. The density of NMP was kept higher than the ultrapure Milli-Q water to allow it to settle down at the bottom of the though, and isopropanol being volatile, left the system. After 30 min, only the composite material remained on the water surface [93], [139]. Clean ITO substrate was clamped to the dipper, and barriers were

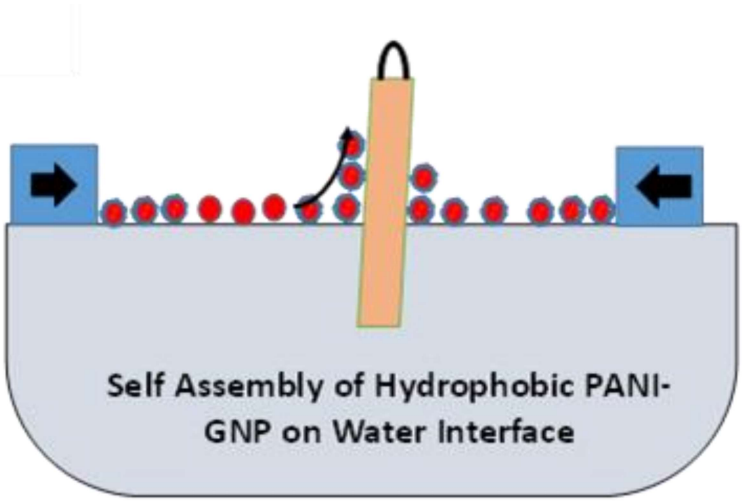

Figure 4.18: *Schematic diagram of LB film deposition process.*

compressed at a speed of 10 mm Min^{-1} to condense the nanocomposite layer on the water surface. LB films were deposited on substrates using vertical dipping at a rate of 2 mm min^{-1} [181]. The depositions were made at a constant pressure of 15 mN m^{-1}, and the deposited film was dried in a vacuum desiccator overnight. To ensure appropriate conditions to achieve complete coverage of the surface with a single layer of the nanocomposite, Langmuir monolayers' pressure-area (p-A) isotherms of PANI-GNP were recorded, and the result is shown in **Figure 4.19**. The available area on the water surface in these isotherms was measured in m^2 with the dispersed quantities of PANI-GNP in mg^{-1}. The PANI-GNP isotherm shows a reduction in surface area from 0.45 to 0.20 m^2/mg, resulting in a linear increase in the pressure from 0 to 19 mN/m as the nanocomposite particles are pushed closer to each other, resulting in small domains. At the same time, the further decrease in the area shows that the compressional elastic modulus has been reached. Beyond the compressional elastic modulus maxima, the nanocomposite particles transition from single layer to multilayer, i.e., tend to overlap. Compressional elastic modulus in the case of PANI-GNP

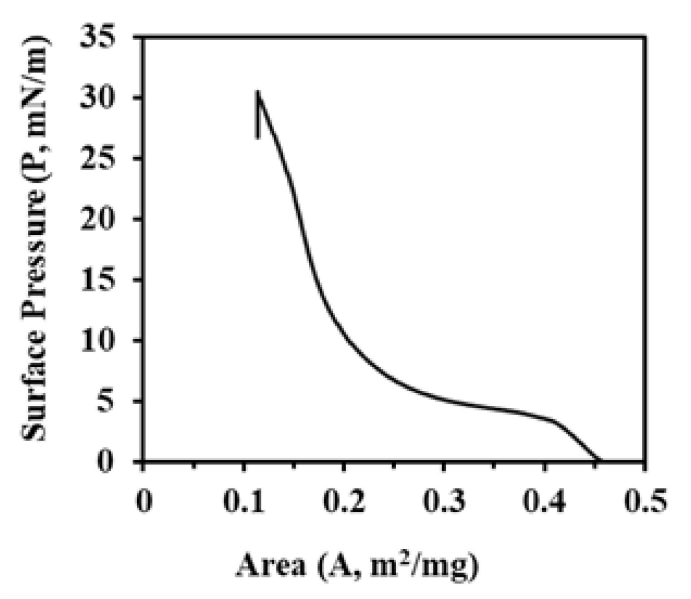

Figure 4.19: *Surface pressure – area (p-A) curve during optimizing of LB film deposition of PANI-GNP.*

nanocomposite sheets are 25 mN/m. Thus, for depositing LB film of PANI-GNP, 15 mN/m pressure was chosen. During this transition, the nanosheets of PANI-GNP float on water due to the hydrophobic nature of PANI-GNP and surface tension, making a sturdy water-air interface. For transferring water-air interface LB films of PANI-GNP on the piranha-treated ITO electrode, having a carboxylic group was clamped to the dipper. Films were deposited on substrates using the vertical dipping method at a speed of 2 mm min^{-1}.

4.4.4 X-ray Photoelectron Spectroscopic Analysis of GNP-PANI film

The change in Au surface state by aniline-assisted electrochemical polymerization was identified using XPS analysis of GNP pre- and post-electropolymerization. XPS elemental analysis of PANI-GNP shows 56.8%, 40.1%, 3.01 %, and 0.5% atomic % proportions of carbon, oxygen, nitrogen, and gold, respectively. The high-resolution X-ray photoelectron spectra of Au4*f* in GNP and PANI-GNP film surfaces are shown in **Figures 4.20 A&B**. The

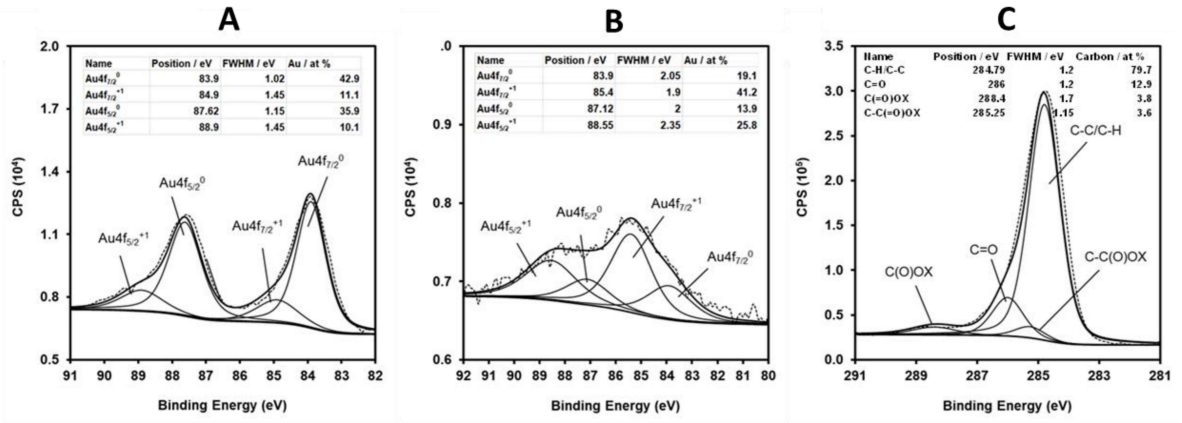

Figure 4.20: *High-resolution Au4f X-ray photoelectron spectra of gold in (A) PANI-GNP film surface, (B) GNP film surface, and (C) C1s X-ray photoelectron spectra of carbon PANI-GNP nanocomposite film surface.*

Au 4*f* spectrum in the PANI-GNP has positive shifts compared to pure GNP [118], or thiol monolayer-protected gold nanoparticles [117], [182]. The analysis showed a multifold increase in positively charged gold as compared to metallic gold in the composite. This positive charge may be attributed due to being the chemisorption of aniline, which has a positively charged functional group that attracts electrons from metallic gold particle surface [183], which also showed a peak shift in Au4 *f* towards the higher binding side [184]. XPS analysis of C1s of PANI-GNP nanocomposite **Figures 4.20 C** does not reveal the presence of a hydroxyl group, suggesting this hydrophobic nature.